arXiv:2005.07892v1 [physics.flu-dyn] 16 May 2020

Prediction of shock wave configurations in compression ramp flows

Yan-Chao Hu[1]†, Wen-Feng Zhou[2], Yan-Guang Yang[3]‡, Zhi-Gong Tang[3] and Zhao-Hu Qin

[1]Hypervelocity Aerodynamics Institute, China Aerodynamics Research and Development Centre, Mianyang 621000, China

[2]State Key Laboratory for Turbulence and Complex Systems and Department of Mechanics,College of Engineering, Peking University, Beijing 100871, China

[3]China Aerodynamics Research and Development Centre, Mianyang 621000, China

(Received xx; revised xx; accepted xx)

Here, we provide a theoretical framework revealing that a steady compression ramp flow must have the minimal dissipation of kinetic energy, and can be demonstrated using the least action principle. For a given inflow Mach number M_0 and ramp angle α, the separation angle θ_s manifesting flow system states can be determined based on this theory. Thus, both the shapes of shock wave configurations and pressure peak p_{peak} behind reattachment shock waves are predictable. These theoretical predictions agree excellently with both experimental data and numerical simulations, covering a wide range of M_0 and α. In addition, for a large separation, the theory indicates that θ_s only depends on M_0 and α, but is independent of the Reynolds number Re and wall temperature T_w. These facts suggest that the proposed theoretical framework can be applied to other flow systems dominated by shock waves, which are ubiquitous in aerospace engineering.

Key words: Authors should not enter keywords on the manuscript.

1. Introduction

Compression ramp flows are canonical complex flows of interactions between shock waves and boundary layers and are ubiquitous in aerospace engineering (Babinsky & Harvey (2011)). As Figure 1 (a) shows, when a large separation occurs, the flow pattern will change significantly, and such a shock pattern was classified as type VI by Edney (1968). In this process, a recirculation region, called a 'separation bubble', will emerge and induce two new shock waves, i.e., the separation and reattachment shock waves. As a result, spatial distributions of physical quantities, such as the flow pressure p, will change. The geometrical features of the separation bubble have a significant contribution that its size (which can be described by the area of the bubble Ω_s) and shape (the separation angle θ_s) determine the range and intensity of the wall pressure p_w, respectively, as shown in Figures 1 (b), (c), and (d). Many numerical (Hung & MacCormack (1976); RUDY *et al.* (1989); Olejniczak & Candler (1998); Deepak *et al.* (2013)) and experimental (Holden (1966); Lewis *et al.* (1968); Délery *et al.* (1986); Mallinson *et al.* (1997)) studies have been conducted and they primarily focused on the size (Burggraf (1975); Rizzetta *et al.*

† Email address for correspondence: yanchaohu@pku.edu.cn
‡ Email address for correspondence: yangyanguang@cardc.cn

(1978); Daniels (1979); Korolev *et al.* (2002)) and internal details (Smith & Khorrami (1991); Korolev *et al.* (2002); Neiland *et al.* (2008); Shvedchenko (2009); Gai & Khraibut (2019)) of the separation bubble. However, only a few of these studies discuss the bubble shape θ_s, even though it is a pivotal parameter in determining the flow field.

Because the emergence of the separation bubble decreases the homogeneity degree of the flow system (symmetry-breaking), the process from the attachment state ($\theta_s = 0$) to the separation state ($\theta_s > 0$), shown in Figure 1 (a), can be analogous to a type of phase transition, where θ_s manifesting the flow states is actually an order parameter — the concept introduced by Landau (1937) for phase transition (see Goldenfeld 2018, pp. 136-137). Therefore, the separation bubble is a 'dissipative structure'—the concept proposed by Prigogine (1978) for structures emerging in systems far from equilibrium—and its self-organization process must be governed by the synergic principle of the subsystems (0,1,2, and 3 that are divided by shock waves and shear layers), shown in Figure 1 (b). From this perspective, this principle is expected to be expressed in an integral form, consisting of the differential governing equation, so that the synergy of this flow system can be described and understood easily. For this purpose, we use the least action principle to establish the equivalent form between the differential and integral scales.

In this paper, we demonstrate that the synergic principle of this flow system is the minimal dissipation theorem. Based on this theorem, the separation angle θ_s can be determined; subsequently, the flow patterns are predictable. The proposed theoretical predictions agree excellently with the numerical and experimental results for a wide range of Mach numbers M_0 and ramp angles α. Additionally, the theorem indicates that shapes of shock wave configurations induced by large separations are independent of the Reynolds number Re and the wall temperature T_w.

2. The minimal dissipation theorem

In this section, we will demonstrate that the flow system has minimal dissipation. The steady states of the flow system satisfy the following equations:

$$\text{mass equation:} \qquad \nabla \cdot (\rho \boldsymbol{u}) = 0 \tag{2.1}$$

$$\text{momentum equation:} \qquad \rho \boldsymbol{u} \cdot \nabla \boldsymbol{u} = \rho \boldsymbol{f} - \nabla p + \nabla(\eta\vartheta) + \nabla \cdot (2\mu \boldsymbol{D}) \tag{2.2}$$

$$\text{kinetic energy equation:} \qquad \rho \boldsymbol{u} \cdot \nabla \left(\frac{1}{2} |\boldsymbol{u}|^2 \right) = \rho \boldsymbol{f} \cdot \boldsymbol{u} + p\vartheta + \nabla \cdot (\boldsymbol{T} \cdot \boldsymbol{u}) - \phi \tag{2.3}$$

where ρ, $\boldsymbol{u}$, $\boldsymbol{f}$, p, η, μ, and $\boldsymbol{q}$ are the density, velocity, body force, pressure, dilatation viscosity, shear viscosity, and heat flux of the flow, respectively. $\vartheta = \nabla \cdot \boldsymbol{u}$, $\boldsymbol{D} = \left[\nabla \boldsymbol{u} + (\nabla \boldsymbol{u})^T\right]/2$, and $\mathbf{T} = (-p + \eta\vartheta)\mathbf{I} + 2\mu\mathbf{D}$ are the velocity divergence, strain-rate tensor, and stress tensor, respectively. ϕ is the dissipation of kinetic energy:

$$\phi = \eta\vartheta^2 + 2\mu \boldsymbol{D} : \boldsymbol{D} \tag{2.4}$$

Helmholtz and Rayleigh (Helmholtz (1868); Rayleigh (1913); Serrin (1959)) proved that, for an incompressible viscous fluid, if the acceleration $\boldsymbol{a} = \boldsymbol{u} \cdot \nabla \boldsymbol{u}$ can be derived by a potential ζ ($\boldsymbol{a} = \nabla\zeta$ or $\nabla \times \boldsymbol{a} = 0$), it should possess minimal dissipation, which is the well-known Helmholtz-Rayleigh minimal dissipation theorem. He *et al.* (1988) generalized this theorem to compressible flows (Wu *et al.* (2007)). Here, we demonstrate the proof process concisely, and provide conditions that compression flows should satisfy. The total dissipation Φ in a control volume V bounded by ℓ is considered, where V is nondeformable or the flow on ℓ (if V is deformable) is nondissipative. With the constraint provided by

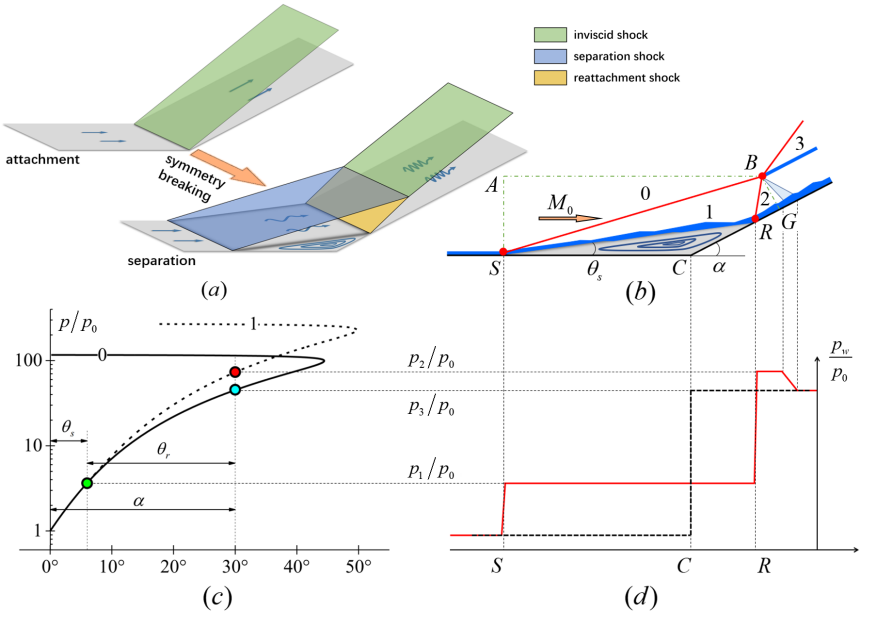


FIGURE 1. (a) Flow patterns of attachment and separation, where inviscid, separation, and reattachment shock waves are green, blue, and orange, respectively; (b) Two types of discontinuity dividing the flow system into four subsystems (0, 1, 2, and 3), where the red and blue parts represent shock waves and shear layers, respectively; (c) Shock polars of this flow system, where polars 0 and 1 correspond to subsystem 0 and 1, respectively. The green, cyan, and red points correspond to p_1/p_0, p_3/p_0 and $p_2/p_0 = p_{peak}/p_0$, respectively; (d) Distributions of wall pressure of flow systems, where the red and black lines correspond to the attachment and separation states, respectively.

Equation (2.1), the variation of Φ can be written as

$$\delta\Phi = \delta \int_V [\phi + \lambda \nabla \cdot (\rho \boldsymbol{u})] dV = 0 \tag{2.5}$$

where λ is a Lagrangian multiplier and $\mathcal{L} = \phi + \lambda \nabla \cdot (\rho \boldsymbol{u})$ is the Lagrangian. Because $\boldsymbol{u}$ and ρ are the two independent variables of $\mathcal{L}$, the Eular-Lagrangian equations are

$$\frac{\delta \mathcal{L}}{\delta \boldsymbol{u}} = 0: \quad \frac{\partial \mathcal{L}}{\partial \boldsymbol{u}} - \nabla \cdot \frac{\partial \mathcal{L}}{\partial \nabla \boldsymbol{u}} - \nabla \frac{\partial \mathcal{L}}{\partial \nabla \cdot \boldsymbol{u}} = 0 \Rightarrow 2[\nabla(\eta\vartheta) + \nabla \cdot (2\mu \boldsymbol{D})] + \rho \nabla \lambda = 0 \tag{2.6}$$

$$\frac{\delta \mathcal{L}}{\delta \rho} = 0: \quad \frac{\partial \mathcal{L}}{\partial \rho} - \nabla \cdot \frac{\partial \mathcal{L}}{\partial \nabla \rho} = 0 \quad \Rightarrow \quad \boldsymbol{u} \cdot \nabla \lambda = 0 \tag{2.7}$$

If a flow satisfies (i) $\boldsymbol{a} = \nabla\zeta$; (ii) $\boldsymbol{f} = -\nabla U$, i.e., the body force can be derived by a potential U; (iii) $\nabla p/\rho = \nabla \int dp/\rho$ or $\nabla p \times \nabla \rho = 0$, i.e., the flow is barotropic, the viscous force can then be derived by a potential ξ from function (2.2), i.e., $[\nabla(\eta\vartheta) + \nabla \cdot (2\mu D)]/\rho = \nabla\xi$. Thus, with λ chosen as $\lambda = -\left(\zeta + \int dp/\rho + U + \xi\right)$, Equations (2.6) and (2.7) can be exactly rearranged to the momentum equation (2.2) and kinetic energy equation (2.3), respectively. Therefore, compressible flows satisfying (i), (ii), and (iii) must have minimal dissipation.

For a flow passing through a straight shock wave, the acceleration $\boldsymbol{a}$ can be decomposed into two parts relative to the shock front, i.e., the vertical component a_n and tangential one a_τ (consider two-dimensional cases). Because $\boldsymbol{u}$ only changes perpendicularly through the shock, there must be $\partial a_n/\partial\tau = 0$ and $a_\tau = 0$, then $|\nabla \times \boldsymbol{a}| = \partial a_\tau/\partial n - \partial a_n/\partial\tau = 0$, satisfying condition (i). Condition (ii) is also satisfied because the body force $\boldsymbol{f}$ is gravity,

which can be negligible. Note that ∇p and $\nabla \rho$ are both perpendicular to the shock front, i.e., $\nabla p \times \nabla \rho = 0$; thus, condition (iii) is satisfied. Therefore, a steady flow across a straight shock wave has minimal dissipation. A corollary of this demonstration is that, if the total dissipation of a steady flow is only contributed by shock waves, this flow should have minimal dissipation. A piece of evidence is that, although two (one weak and one strong) oblique shock waves are both theoretically possible for the same deflection angle, the observable shock wave, in practice, is always the weak one.

3. Dissipation of the flow system

In this section, we will demonstrate that, for a large separation, the total dissipation Φ of this flow system is primarily contributed by shock waves, and show the dependency of Φ on θ_s.

As 1 (b) shows, four types of flow structure probably generate dissipation, i.e., (i) shock waves, (ii) shear layers, (iii) the separation bubble, and (iv) the expansion fan (behind the triple point B). For (i), a shock wave with length L_ω, the dissipation can be estimated as $\int_{L_\omega}\int_{\epsilon_\omega} \phi dn d\tau \sim \mathcal{O}(\mu_\omega \Delta u_\omega^2 L_\omega/\epsilon_\omega)$ using Equation (2.4), where L_ω, ϵ_ω, μ_ω, and Δu_ω are the characteristic length, thickness, viscosity, and velocity difference of this shock, respectively. For (ii), a shear layer with length L_δ, its dissipation can also be estimated, i.e., $\int_{L_\delta}\int_{\epsilon_\delta} \phi dn d\tau \sim \mathcal{O}(\mu_\delta \Delta u_\delta^2 L_\delta/\epsilon_\delta)$, where ϵ_δ, μ_δ, and Δu_δ are the characteristic thickness, viscosity, and velocity difference of this shear layer, respectively. Because $\mu_\delta \sim \mu_\omega$, $\Delta u_\delta \sim \Delta u_\omega$, $L_\delta \sim L_\omega$, and $\epsilon_\delta \gg \epsilon_\omega$, dissipations induced by shear layers are negligible relative to those induced by shock waves. For (iii), a separation bubble Ω_s with characteristic length L_s (i.e., $L_s^2 \sim \mathcal{O}(\Omega_s)$), its dissipation can be estimated as $\int_{\Omega_s} \phi dV \sim \mathcal{O}(\mu_s \Delta u_s^2)$, where μ_s is the characteristic viscosity of the bubble. Although its internal vortex structure may be complex, its characteristic velocity Δu_s is always very small relative to Δu_ω, i.e., $\Delta u_s \ll \Delta u_\omega$. In consideration of $L_\omega/\epsilon_\omega \gg 1$, the dissipation induced by the separation bubble can be negligible as well. For (iv), an expansion fan with area Ω_f, its dissipation $\int_{\Omega_f} \phi dV$ can be calculated using the relation $\phi = \rho T ds/dt - \nabla \cdot \boldsymbol{q}$, i.e., the deformation of the energy equation (Wu *et al.* (2007)), where ds/dt, T, and $\boldsymbol{q}$ are the entropy production, temperature, and heat conductivity of the flow, respectively. Because the flow passing through Ω_f is an isentropic process, and the heat flux $\boldsymbol{q}$ on the boundary $\partial\Omega_f$ of Ω_f is zero, there must be $\int_{\Omega_f}(\rho T ds/dt - \nabla \cdot \boldsymbol{q}) dV = 0$. Therefore, the dissipation induced by the expansion fan is zero. In this flow system, the appropriate control volume V is chosen and is bounded by AB, BG, GC, CS and SA, as shown in Figure 1 (b). Because the total dissipation in V is primarily contributed by shock waves SB and RB, a steady flow in V should have minimal dissipation, which implies θ_s of a steady state should cause shock waves SB and RB to dissipate minimal kinetic energy.

Subsequently, we will illustrate how the total dissipation Φ depends on θ_s. By integrating function (2.3) across the shock wave perpendicularly, we obtain the dissipation induced by a shock wave per unit length:

$$
\begin{aligned}
\widehat{\phi} &= \int_{\epsilon_\omega} \phi dn = \mathcal{E} - \mathcal{P} \\
\mathcal{E} &= -\int_{\epsilon_\omega} \rho \boldsymbol{u} \cdot \nabla \left(\frac{1}{2}|\boldsymbol{u}|^2 \right) dn = \frac{1}{2}\left\{ \rho_a \left(M_a c_a \sin\beta \right)^3 - \rho_b \left[M_b c_b \sin\left(\beta - \theta\right) \right]^3 \right\} \\
\mathcal{P} &= -\int_{\epsilon_\omega} p\vartheta dn \approx \frac{1}{2}\left(p_a + p_b \right) \left[M_a c_a \sin\beta - M_b c_b \sin\left(\beta - \theta\right) \right]
\end{aligned}
\tag{3.1}
$$

where $\mathcal{E}$ and $\mathcal{P}$ are the kinetic energy loss and the negative work of pressure, respectively, implying that one portion of the kinetic energy loss is stored as the potential energy and the other is dissipated. In Equation (3.1), M, c, and β are the Mach number, acoustic velocity, and shock angle, respectively. The subscripts 'a' and 'b' are the locations ahead of and behind a shock wave, respectively. As 1 (b) shows, 'a' and 'b' correspond to '0' and '1' for shock SB, and to '1' and '2' for RB, respectively. Quantities in Equation (3.1) satisfy the following:

$$\left.\begin{array}{ll} M_1^2 = \mathcal{F}_M\left(M_0, \beta_s\right), & M_2^2 = \mathcal{F}_M\left(M_1, \beta_r\right) \\ c_0/c_1 = \mathcal{F}_c\left(M_0, \beta_s\right), & c_1/c_2 = \mathcal{F}_c\left(M_1, \beta_r\right) \\ \rho_0/\rho_1 = \mathcal{F}_\rho\left(M_0, \beta_s\right), & \rho_1/\rho_2 = \mathcal{F}_\rho\left(M_1, \beta_r\right) \\ p_0/p_1 = \mathcal{F}_p\left(M_0, \beta_s\right), & p_1/p_2 = \mathcal{F}_p\left(M_1, \beta_r\right) \\ \mathcal{F}_\beta\left(M_0, \beta_s, \theta_s\right) = 0, & \mathcal{F}_\beta\left(M_1, \beta_r, \theta_r\right) = 0 \\ \theta_r = \alpha - \theta_s & \end{array}\right\} \tag{3.2}$$

where β_s and β_r are the shock angles of SB and RB, respectively, and θ_r is the deflection angle of the flow across RB. $\mathcal{F}_M$, $\mathcal{F}_c$, $\mathcal{F}_\rho$, $\mathcal{F}_p$, and $\mathcal{F}_\beta$ are the classical Rankine-Hugoniot relations (Rankine (1870, 1887)):

$$\begin{aligned} \mathcal{F}_M(M,\beta) &\equiv \frac{M^2 + \frac{2}{\gamma-1}}{\frac{2\gamma}{\gamma-1}M^2\sin^2\beta - 1} + \frac{M^2\cos^2\beta}{\frac{\gamma-1}{2}M^2\sin^2\beta + 1} \\ \mathcal{F}_c(M,\beta) &\equiv \frac{\left[(\gamma-1)M^2\sin^2\beta + 2\right]^{1/2}\left[2\gamma M^2\sin^2\beta - (\gamma-1)\right]^{1/2}}{(\gamma+1)M\sin\beta} \\ \mathcal{F}_\rho(M,\beta) &\equiv \frac{(\gamma+1)M^2\sin^2\beta}{(\gamma-1)M^2\sin^2\beta + 2}, \quad \mathcal{F}_p(M,\beta) \equiv \frac{2\gamma}{\gamma+1}M^2\sin^2\beta - \frac{\gamma-1}{\gamma+1} \\ \mathcal{F}_\beta(M,\beta,\theta) &\equiv 2\cot\beta\frac{M^2\sin^2\beta - 1}{M^2(\gamma+\cos 2\beta) + 2} - \tan\theta \end{aligned} \tag{3.3}$$

Therefore, for a given inflow Mach number M_0 and ramp angle α, both $\widehat{\phi}_{ST}$ and $\widehat{\phi}_{RT}$ depend only on the order parameter θ_s. We will now show the geometrical relationships of the flow system. For a large separation, the size (area) of the separation bubble Ω_s can be calculated using the triangle area formula:

$$\Omega_s = \frac{L_{SR}^2\sin\theta_r\sin\theta_s}{2\sin\alpha} \tag{3.4}$$

where L_{SR} is the length of the free shear layer starting from the separation point S to the reattachment point R. Note that the flow at a low velocity in the separation bubble is approximately incompressible, where the pressure, temperature, and density are $p_1(\theta_s)$, T_w, and $\rho_s(\theta_s) = \gamma M_0^2 p_1(\theta_s)/T_{wall}$, respectively. Considering that a stronger adverse pressure gradient can press more flows into the separation bubble, we assume that $\mathit{\Pi}_s(\theta_s) \propto p_1(\theta_s)/p_0$ as θ_s varies, where $\mathit{\Pi}_s(\theta_s) = \rho_s(\theta_s)\Omega_s$ is the mass of the flow in the bubble. Thus, $\Omega_s \propto T_{\text{wall}}/\left(\rho_0 T_0\right)$ remains constant as θ_s varies. By normalizing formula (3.4) with Ω_s, we obtain

$$\ell_{SR} = \sqrt{\frac{2\sin\alpha}{\sin\theta_r\sin\theta_s}} \tag{3.5}$$

where ℓ_{SR} is the dimensionless length of L_{SR} being nondimensionalized using $\sqrt{\Omega_s}$. The

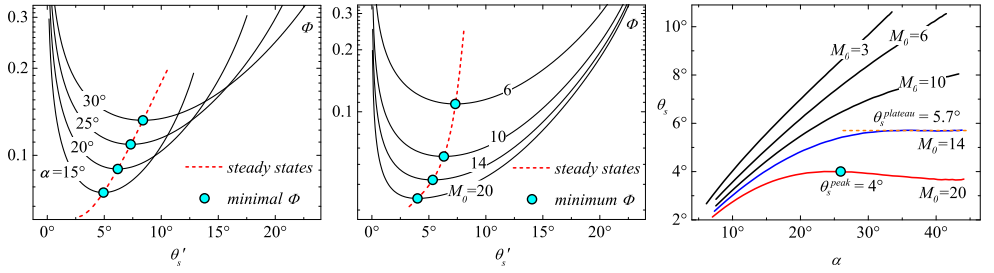


FIGURE 2. Theoretical θ_s corresponding to minimal dissipation. (a) and (b) depict Φ at all possible θ_s', where the cyan points are the minimal dissipation, and the red dash lines are the theoretical prediction results. (a) $\alpha = 15, 20, 25$, and 30° with $M_0 = 6$; (b) $M_0 = 20, 14, 10$, and 6 at $\alpha = 25^\circ$. (c) Theoretical θ_s varying with α at different M_0.

coordinate of point S is set as $(0, 0)$; thus points B and R are

$$\begin{aligned} x_B &= \ell_{SR}\frac{\sin\theta_s - \cos\theta_s\tan(\beta_r+\theta_s)}{\tan\theta_s - \tan(\beta_r+\theta_s)}, y_B = x_B\tan\beta_s \\ x_R &= \ell_{SR}\cos\theta_s, y_R = \ell_{SR}\sin\theta_s \end{aligned} \tag{3.6}$$

Thus, the lengths of shock wave SB and RB can be obtained:

$$\begin{aligned} \ell_{SB} &= \sqrt{x_B^2 + y_B^2} \\ \ell_{RB} &= \sqrt{(x_B - x_R)^2 + (y_B - y_R)^2} \end{aligned} \tag{3.7}$$

Using Equations (3.1) and (3.7), we can calculate the total dissipation Φ in V:

$$\Phi(\theta_s) = \widehat{\phi}_{SB}\ell_{SB} + \widehat{\phi}_{RB}\ell_{RB} \tag{3.8}$$

4. Results

Figure 2 (a) and (b) depict the variation of the total dissipation Φ with all possible separation angle θ_s', where (a) depicts Φ at different ramp angles α with inflow Mach number $M_0 = 6$, and (b) depicts Φ with different M_0 at $\alpha = 25^\circ$. As demonstrated in **Sections 2** and **3**, steady states of the flow system must have minimal dissipation. Therefore, if a steady state is at θ_s, there must be

$$\left.\frac{\partial\Phi}{\partial\theta_s'}\right|_{\theta_s} = 0, \quad \left.\frac{\partial^2\Phi}{\partial\theta_s'^2}\right|_{\theta_s} > 0 \tag{4.1}$$

Only one minimal value of Φ can be observed to exist for a given M_0 and α, indicating that only one steady state exists in a compression ramp with large separation, which corresponds with all experimental observations. Figure 2(c) shows the variation in the theoretical θ_s with different M_0 and α. For a given α, θ_s is observed to decrease as M_0 increases. However, for a given M_0, three possible scenarios occur, i.e., (i) θ_s increases with α ($M_0 = 3, 6, 10$); (ii) θ_s increases when α is moderate but maintains at a plateau when α is sufficiently large (for $M_0 = 14$, $\theta_s \approx 5.7^\circ$ when $\alpha > 35^\circ$); (iii) there is a critical α corresponding to a peak θ_s (for $M_0 = 20$, critical $\alpha \approx 26^\circ$ and $\theta_s^{peak} \approx 4^\circ$), over which θ_s will decrease as α increases.

Figure 3 shows the comparison of the proposed theoretical θ_s, β_s, and β_r with numerical results from different researchers (our DNSs, Babinsky & Harvey (2011, pp. 318-319) and

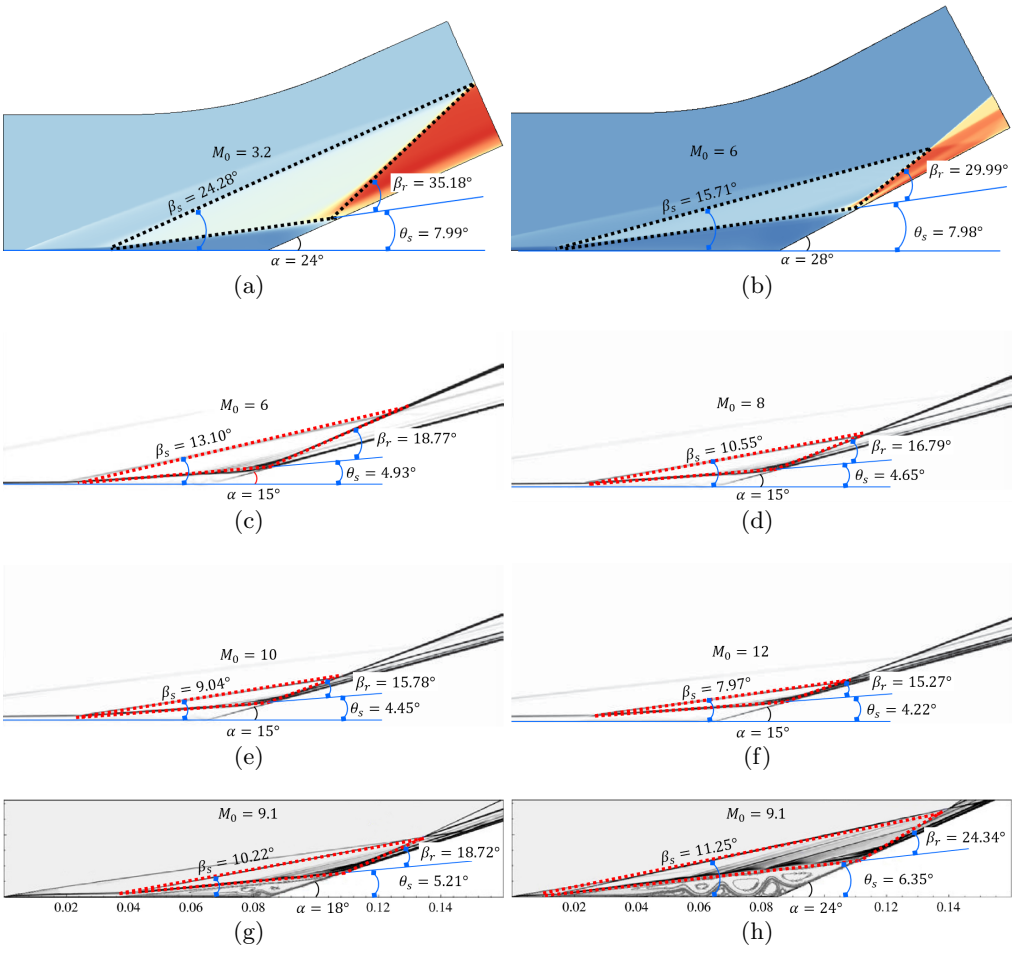


FIGURE 3. Comparison of the proposed theoretical θ_s, β_s and β_r (dash line) with numerical results. We simulated (a) $M_0 = 3.2$ and $\alpha = 24°$ and (b) $M_0 = 6$ and $\alpha = 28°$ and coloured them by density contours; (c)–(f) are extracted from Babinsky & Harvey (2011, pp. 318-319) at $\alpha = 15°$, where (c) $M_0 = 6$, (d) $M_0 = 8$, (e) $M_0 = 10$, and (f) $M_0 = 12$; (g) and (h) are extracted from Gai & Khraibut (2019) with $M_0 = 9.1$, where (g) $\alpha = 18°$ and (h) $\alpha = 24°$.

Gai & Khraibut (2019)). The theory in this paper can be observed to agree well with the flow patterns encompassing a wide range of Mach numbers and ramp angles (M_0 varying from 3.2 to 12, α varying from 15 to 28°). As M_0 and α increase, the pressure peak p_{peak} behind the reattachment shock wave, located at subsystem 2 in Figure 1 (b), increases rapidly and will be two orders of magnitude larger than the free-stream pressure p_0. Figure 4 depicts the comparison of theoretical p_{peak} with that of previous works, including experimental ((Holden 1970; Elfstrom 1972; Delery & Coet 1990, 1991)) and numerical (RUDY *et al.* (1989); Jiang & Richards (1991); Thomas *et al.* (1991); Vahdati *et al.* (1991); Mallet *et al.* (1991); Chalot *et al.* (1991); Simeonides *et al.* (1994); Simeonides & Haase (1995); Marini (2001); Babinsky & Harvey (2011); Gai & Khraibut (2019)) results. The theoretical p_{peak}/p_0 is observed to agree well with all the numerical and experimental results with a M_0 varying from 3.2 to 14.1 and α varying from 15 to 38°. Furthermore, for a large separation, as Table 1 shows, the theoretical predictions

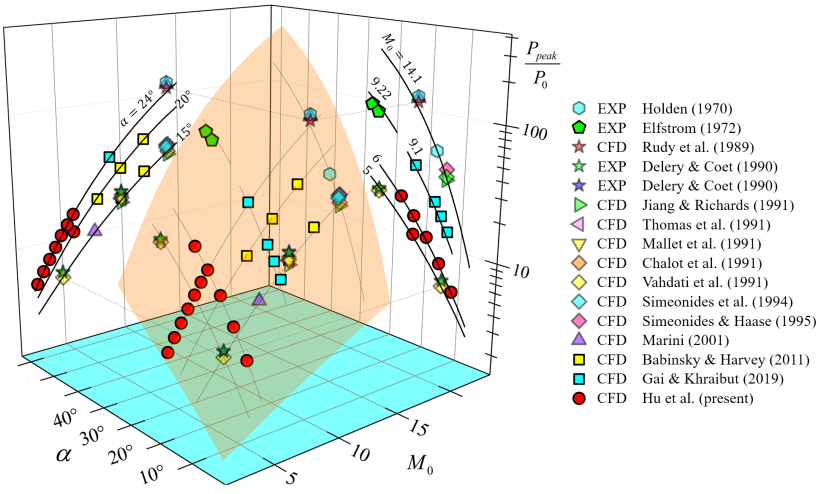


FIGURE 4. Comparison of theoretical pressure peak p_{peak} with numerical and experimental results. The three-dimensional orange surface is the solution of p_{peak}/p_0 depending on both M_0 and α. The thick black lines on the (M_0,p_{peak}/p_0)-plane and (α,p_{peak}/p_0)-plane are projections of the thin ones on the theoretical p_{peak}/p_0-surface.

M_0	α	Re_0 (m^{-1})	T_w (K)	T_0 (K)	state	p_{peak}/p_0 theory	p_{peak}/p_0 EXP/CFD	p_3/p_0 inviscid	author
14.1	24°	2.362×10^5	297.22	88.88	L	102.95	123.5 (EXP)	58.02	Holden
14.1	18°	2.362×10^5	297.22	88.88	L	54.52	51.88 (EXP)	34.23	
9.22	38°	$4 \times 10^5 (Re_{L_\delta})$	295	59.44	T	106.08	93.13 (EXP)	58.28	Elfstrom
9.1	24°	3.22×10^6	351.24	160	L	36.3	37.32 (CFD)	25.48	Gai & Khraibut
6.0	28°	2.79×10^6	307	108.1	L	20.04	20.15 (CFD)	15.84	Hu et al.

TABLE 1. Comparison of theoretical pressure peak p_{peak} with numerical and experimental results for five conditions encompassing different Reynolds numbers and wall temperature. Re_{L_δ} is the Reynolds number of the boundary layer in the upstream of the separation point, of which the characteristic thickness is L_δ, and the states 'L' and 'T' are laminar and turbulent, respectively. p_3/p_0 is the pressure rise of the flows through the inviscid shock wave.

are independent of the the Reynolds number Re and the wall temperature T_w, which is because the dissipation induced by shear layers can be negligible relative to shock waves, as demonstrated in **Section 3**. Additionally, as the maximum heat flux h_{peak} generated in the reattachment region can be correlated with p_{peak} in terms of simple power-law relations (Holden (1978)), the proposed theory can be used to estimate the h_{peak} quantificationally, which is vital in both supersonic and hypersonic flows.

5. Conclusion

In this work, the least action principle is used to reveal that the synergic principle of a compression ramp flow with large separation is the minimal dissipation theorem. Based on this theorem, we obtain theoretical flow patterns and the pressure peak p_{peak}, which agree very well with the numerical and experimental results for a wide range of Mach numbers M_0 and ramp angles α. Because the maximum heat flux h_{peak} at the

reattachment region can be correlated with p_{peak} in terms of simple power-laws, h_{peak} can be estimated quantificationally, which is vital in aerospace engineering. Furthermore, the predicted results are independent of the Reynolds number Re and wall temperature T_w. The present theoretical framework has both a strict mathematical logic and a clear physical image, which are expected to be applied to other flow systems dominated by shock waves.

Acknowledgement

We are grateful to Professor You-Sheng Zhang for his helpful discussion and to Professor Xin-Liang Li for his support of the numerical simulation. This work is supported by National Key R & D Program of China (Grant No.2019YFA0405300).

REFERENCES

Babinsky, Holger & Harvey, John K 2011 *Shock wave-boundary-layer interactions*, , vol. 32. Cambridge University Press.

Burggraf, OR 1975 Asymptotic theory of separation and reattachment of a laminar boundary layer on a compression ramp. *Tech. Rep.*. OHIO STATE UNIV RESEARCH FOUNDATION COLUMBUS.

Chalot, F, Hughes, TJR, Johan, Z & Shakib, F 1991 Application of the galerkin/least-squares formulation to the analysis of hypersonic flows: I. flow over a two-dimensional ramp. In *Hypersonic Flows for Reentry Problems*, pp. 181–200. Springer.

Daniels, PG 1979 Laminar boundary-layer reattachment in supersonic flow. *Journal of Fluid Mechanics* **90** (2), 289–303.

Deepak, NR, Gai, SL & Neely, AJ 2013 A computational investigation of laminar shock/wave boundary layer interactions. *The Aeronautical Journal* **117** (1187), 27–56.

Delery, J & Coet, MC 1990 Experimental investigation of shock-wave boundary-layer interaction in hypersonic flows. In *Workshop on Hypersonic Flows for Reentry Problems*, , vol. 3, pp. 1–22.

Delery, J & Coet, M-C 1991 Experiments on shock-wave/boundary-layer interactions produced by two-dimensional ramps and three-dimensional obstacles. In *Hypersonic Flows for Reentry Problems*, pp. 97–128. Springer.

Délery, Jean, Marvin, John G & Reshotko, Eli 1986 Shock-wave boundary layer interactions. *Tech. Rep.*. ADVISORY GROUP FOR AEROSPACE RESEARCH AND DEVELOPMENT NEUILLY-SUR-SEINE (FRANCE).

Edney, Barry 1968 Anomalous heat transfer and pressure distributions on blunt bodies at hypersonic speeds in the presence of an impinging shock. *Tech. Rep.*. Flygtekniska Forsoksanstalten, Stockholm (Sweden).

Elfstrom, GM 1972 Turbulent hypersonic flow at a wedge-compression corner. *Journal of fluid Mechanics* **53** (1), 113–127.

Gai, Sudhir L & Khraibut, Amna 2019 Hypersonic compression corner flow with large separated regions. *Journal of Fluid Mechanics* **877**, 471–494.

Goldenfeld, Nigel 2018 *Lectures on phase transitions and the renormalization group*. CRC Press.

He, Ke-Ren, Yang, D-H & Wu, Jie-Zhi 1988 The extension of minimum energy dissipation theorem and limitation of minimum entropy production principle in fluid flow (in chinese). *J. Engng. Thermophys* **9**, 1012.

Helmholtz, H von 1868 Zur theorie der stationären ströme in reibenden flüssigkeiten. *Wiss. Abh* **1**, 223–230.

Holden, Michael 1978 A study of flow separation in regions of shock wave-boundary layer interaction in hypersonic flow. In *11th Fluid and PlasmaDynamics Conference*, p. 1169.

Holden, Michael S 1966 Experimental studies of separated flows at hypersonic speeds. ii-two-dimensional wedge separated flow studies. *AIAA Journal* **4** (5), 790–799.

Holden, Michael S 1970 Theoretical and experimental studies of the shock wave-boundary

layer interaction on compression surfaces in hypersonic flow. *Tech. Rep.*. CORNELL AERONAUTICAL LAB INC BUFFALO NY.

Hung, CM & MacCormack, RW 1976 Numerical solutions of supersonic and hypersonic laminar compression corner flows. *AIAA Journal* **14** (4), 475–481.

Jiang, Dachun & Richards, BE 1991 Hypersonic viscous flow over two-dimensional ramps. In *Hypersonic Flows for Reentry Problems*, pp. 228–243. Springer.

Korolev, GL, Gajjar, JSB & Ruban, AI 2002 Once again on the supersonic flow separation near a corner. *Journal of Fluid Mechanics* **463**, 173–199.

Landau, Lev Davidovich 1937 On the theory of phase transitions. *Ukr. J. Phys.* **11**, 19–32.

Lewis, John E, Kubota, Toshi & Lees, Lester 1968 Experimental investigation of supersonic laminar, two-dimensional boundary-layer separation in a compression corner with and without cooling. *AIAA journal* **6** (1), 7–14.

Mallet, M, Mantel, B, Périaux, J & Stoufflet, B 1991 Contribution to problem 3 using a galerkin least square finite element method. In *Hypersonic Flows for Reentry Problems*, pp. 255–267. Springer.

Mallinson, SG, Gai, SL & Mudford, NR 1997 The interaction of a shock wave with a laminar boundary layer at a compression corner in high-enthalpy flows including real gas effects. *Journal of fluid mechanics* **342**, 1–35.

Marini, Marco 2001 Analysis of hypersonic compression ramp laminar flows under sharp leading edge conditions. *Aerospace science and technology* **5** (4), 257–271.

Neiland, V Ya, Sokolov, LA & Shvedchenko, VV 2008 Temperature factor effect on the structure of the separated flow within a supersonic gas stream. *Fluid Dynamics* **43** (5), 706–717.

Olejniczak, Joseph & Candler, Graham 1998 Computation of hypersonic shock interaction flow fields. In *7th AIAA/ASME Joint Thermophysics and Heat Transfer Conference*, p. 2446.

Prigogine, Ilya 1978 Time, structure, and fluctuations. *Science* **201** (4358), 777–785.

Rankine, PH 1887 Sur la propagation du mouvement dans les corps et spécialement dans les gaz parfaits, 2e partie. *Journal de lÉcole Polytechnique. Paris* **57**, 3–97.

Rankine, William John Macquorn 1870 Xv. on the thermodynamic theory of waves of finite longitudinal disturbance. *Philosophical Transactions of the Royal Society of London* (160), 277–288.

Rayleigh, Lord 1913 Lxv. on the motion of a viscous fluid. *The London, Edinburgh, and Dublin Philosophical Magazine and Journal of Science* **26** (154), 776–786.

Rizzetta, DP, Burggraf, OR & Jenson, Richard 1978 Triple-deck solutions for viscous supersonic and hypersonic flow past corners. *Journal of Fluid Mechanics* **89** (3), 535–552.

RUDY, DAVID, THOMAS, JAMES, Kumar, Ajay, GNOFF, PETER & CHAKRAVARTHY, SUKUMAR 1989 A validation study of four navier-stokes codes for high-speed flows. In *20th Fluid Dynamics, Plasma Dynamics and Lasers Conference*, p. 1838.

Serrin, James 1959 Mathematical principles of classical fluid mechanics. In *Fluid Dynamics I/Strömungsmechanik I*, pp. 125–263. Springer.

Shvedchenko, Vladimir Viktorovich 2009 About the secondary separation at supersonic flow over a compression ramp. *TsAGI Science Journal* **40** (5).

Simeonides, G & Haase, W 1995 Experimental and computational investigations of hypersonic flow about compression ramps. *Journal of Fluid Mechanics* **283**, 17–42.

Simeonides, G, Haase, W & Manna, M 1994 Experimental, analytical, and computational methods applied to hypersonic compression ramp flows. *AIAA journal* **32** (2), 301–310.

Smith, FT & Khorrami, A Farid 1991 The interactive breakdown in supersonic ramp flow. *Journal of fluid mechanics* **224**, 197–215.

Thomas, James L, Rudy, David H, Kumar, Ajay & Van Leer, Bram 1991 Grid-refinement study of hypersonic laminar flow over a 2-d ramp. In *Hypersonic Flows for Reentry Problems*, pp. 244–254. Springer.

Vahdati, M, Morgan, K & Peraire, J 1991 The application of an adaptive upwind unstructured grid solution algorithm to the simulation of compressible laminar viscous flows over compression corners. In *Hypersonic Flows for Reentry Problems*, pp. 201–211. Springer.

Wu, Jie-Zhi, Ma, Hui-Yang & Zhou, M-D 2007 *Vorticity and vortex dynamics*. Springer Science & Business Media.